Interlayer screening effect in graphene multilayers with *ABA* and *ABC* stacking

Mikito Koshino
Department of Physics, Tokyo Institute of Technology, 2-12-1 Ookayama, Meguro-ku, Tokyo 152-8551, Japan
(Received 6 November 2009; revised manuscript received 17 January 2010; published 4 March 2010)

We study the effect of perpendicular electric fields on the band structures of *ABA* and *ABC* graphene multilayers, and find that the electronic screening effect is significantly different between them. In *ABA* multilayers, the field produces a band overlap and gives a linear screening, while in *ABC* multilayers, in contrast, it opens an energy gap in the surface-state band at low energy, leading to a strong screening effect essentially nonlinear to the field amplitude. The energy gap of a large *ABC* stack sharply rises when the external field exceeds a certain critical value.

DOI: 10.1103/PhysRevB.81.125304 PACS number(s): 73.22.−f, 73.21.−b, 73.61.−r

I. INTRODUCTION

Recent experimental realizations of atomically thin graphene systems[1–3] open up possibilities of exploring their exotic electronic properties. In multilayer films composed of more than two graphene layers, the interlayer coupling strongly modifies the linear dispersion of monolayer graphene, resulting in various electronic structures depending on the number of layers, N.[4–22] The band structure can also be changed by applying a gate electric field perpendicular to the layer through generating an interlayer potential asymmetry. In bilayer graphene, for example, an energy gap opens between the conduction and valence bands in presence of gate electric field[7,10,12,20,23–27] and it was actually observed in transport[28,29] and spectroscopic measurements.[5,6,30–34]

In nature, there are two known forms of bulk graphite called *ABA* (*AB*, hexagonal, or Bernal) and *ABC* (rhombohedral) with different stacking manners as shown in Fig. 1. The *ABA* phase is thermodynamically stable and common while it is known that some portion of natural graphite takes the *ABC* form.[35] For *ABA* graphite, the effective-mass model describing the electronic property was developed for the bulk system[36–42] and also for few-layer systems.[7–10,12–18] The energy dispersion of the multilayer graphenes includes the subbands analog to monolayer or the bilayer graphene,[10,13] and the Hamiltonian is actually decomposed into independent subsystems effectively identical to monolayer or bilayer.[14,16] The *ABC* graphite has a quite different electronic structure from *ABA*'s.[10,11,26,43–49] In particular, the low-energy band of a finite *ABC* multilayer are given by the surface states localized at outermost layers,[10,15] and the interlayer potential asymmetry opens an energy gap in those bands.[26,46,49] This is in sharp contrast with *ABA* multilayers where potential asymmetry causes a band overlapping.[18,26]

In considering the interlayer potential asymmetry induced by an external electric field, it is essential to take into account screening effect, as done in bilayer graphene,[23–25] and *ABA* multilayers.[18,20,50] Experimentally, the interlayer screening effect in the gate electric field was probed in thin graphite films.[6,51–53] Here we calculate the self-consistent band structure of *ABA* and *ABC* multilayers with various N's in the presence of perpendicular electric field. For *ABA* multilayers, we show that the electric field generally produces band overlapping, and the screening is shown to be linear to the field amplitude. In *ABC* multilayers, on the other hand, the low-energy surface band causes a strong nonlinear screening effect through opening an energy gap. The paper is organized as follows: we present the effective-mass models for *ABA* and *ABC* multilayers in Sec. II and compute the band structure including the self-consistent screening effect in Sec. III. The conclusion is given in Sec. IV

II. EFFECTIVE HAMILTONIAN AND BAND STRUCTURE

A. *ABA* multilayers

We first consider a multilayer graphene with *ABA* stacking composed of N layers of a graphene layers. We label A and B on ith layer as A_i and B_i. In *ABA* stacking, the sites $B_1, A_2, B_3, A_4, \ldots$ are arranged along vertical columns normal to the layer plane, while the rest sites $A_1, B_2, A_3, B_4, \ldots$ are above or below the center of hexagons in the neighboring layers, as shown in Fig. 1(a). The system is described by a $\mathbf{k}\cdot\mathbf{p}$ Hamiltonian based on three-dimensional (3D) graphite

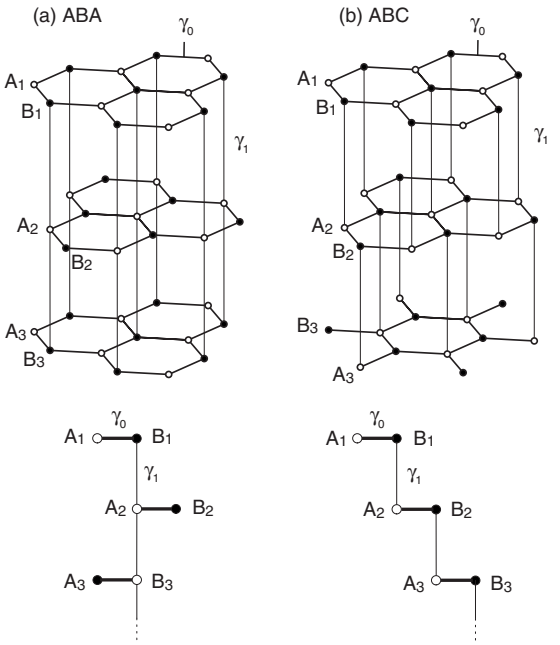

FIG. 1. Atomic structures of multilayer graphenes with (a) *ABA* (Bernal) stacking and (b) *ABC* (rhombohedral) stacking

model.[36–42] As the simplest approximation, we include parameter γ_0 describing the nearest-neighbor coupling within each layer, and γ_1 for the coupling of the interlayer vertical bonds. The band parameters were experimentally estimated in the bulk *ABA* graphite, for example,[42] as $\gamma_0=3.16$ eV and $\gamma_1=0.39$ eV, which we will use in the following calculations. The lattice constant of honeycomb lattice (distance between nearest *A* atoms) is given by $a=0.246$ nm and the interlayer spacing $d=0.334$ nm.

The low-energy spectrum is given by the states in the vicinity of K and K' points in the Brillouin zone. Let $|A_j\rangle$ and $|B_j\rangle$ be the Bloch functions at the K point, corresponding to the A and B sublattices, respectively, of layer j. If the basis is taken as $|A_1\rangle,|B_1\rangle;\ |A_2\rangle,|B_2\rangle;\ldots;\ |A_N\rangle,|B_N\rangle$, the Hamiltonian around the K point is given by[10,12–14]

$$\mathcal{H}_{ABA}=\begin{pmatrix} H_1 & V & & & \\ V^\dagger & H_2 & V^\dagger & & \\ & V & H_3 & V & \\ & & \ddots & \ddots & \ddots \end{pmatrix}, \tag{1}$$

and

$$H_j=\begin{pmatrix} U_j & vp_- \\ vp_+ & U_j \end{pmatrix}, \quad V=\begin{pmatrix} 0 & 0 \\ \gamma_1 & 0 \end{pmatrix}, \tag{2}$$

where U_j is the electrostatic potential at jth layer, and we defined $p_\pm=p_x\pm ip_y$ with $\boldsymbol{p}=-i\hbar\nabla$. v is the band velocity of monolayer graphene given by $v=\sqrt{3}a\gamma_0/2\hbar$. The effective Hamiltonian for another valley, K', is obtained by interchanging p_+ and p_-.[7]

When $U_j=0$, Hamiltonian (1) can be decomposed into subsystems identical to bilayer or monolayer graphenes with a basis appropriately chosen.[14] The subsystems are labeled by an index m which ranges as

$$m=\begin{cases} 1,3,5,\ldots,N-1 & N=\text{even} \\ 0,2,4,\ldots,N-1 & N=\text{odd}. \end{cases} \tag{3}$$

The eigenenergies at $U_j=0$ are given[10,14] for $m=0$ as $\varepsilon^{ABA}_{m=0,s}(p)=svp$, and for $m\neq 0$ as

$$\varepsilon^{ABA}_{m,\mu,s}(p)=s[\mu\gamma_1\cos\kappa_m+\sqrt{(\gamma_1\cos\kappa_m)^2+(vp)^2}], \tag{4}$$

where $p=\sqrt{p_x^2+p_y^2}$, $\mu=\pm$, $s=\pm$, and

$$\kappa_m=\frac{\pi}{2}-\frac{m\pi}{2(N+1)}. \tag{5}$$

$m=0$ only exists in odd-layer graphene and gives an energy band identical to monolayer graphene. Other m's are bilayer-type band structures where $\mu=-$ gives a pair of electron ($s=+$) and hole bands ($s=-$) touching at zero energy, and $\mu=+$ another pair repelled away by $\pm 2\gamma_1\cos\kappa_m$. The dispersion around $k=0$ is approximately quadratic with the effective mass[7]

$$m^*=\frac{\gamma_1}{v^2}\cos\kappa_m, \tag{6}$$

giving the density of states at zero energy, $\rho_m=g_vg_sm^*/(2\pi\hbar)$, with $g_v=2$ and $g_s=2$ are valley (K,K') and spin degeneracies, respectively.

The quantity κ_m corresponds to the wave number k_z in the layer stacking direction (z direction) via $\kappa_m=k_zd$.[10,14] The wave function of subband m is indeed a standing wave in z direction with wave number κ_m. The total density of states per layer, $\bar{\rho}=(1/N)\Sigma_m\rho_m$, approximates in large-$N$ limit,

$$\bar{\rho}=g_vg_s\frac{\gamma_1}{2\pi^2\hbar^2v^2}, \tag{7}$$

where Σ_m is replaced with integration in κ.

B. *ABC* multilayers

The *ABC* multilayer have a different arrangement shown in Fig. 1(b), where vertical bonds couple the pairs (B_j,A_{j+1}) for $j=1,2,\ldots,N-1$. We use the same notation γ_0 and γ_1 as in *ABA* graphite, for the nearest intralayer and interlayer coupling, respectively. Although the band parameters are not identical between *ABA* and *ABC* graphites, we refer to the values of *ABA* in the following numerical calculations, assuming that the corresponding coupling parameters have similar values.[44] Hamiltonian around the K point can be written as[10,44,45,48]

$$\mathcal{H}_{ABC}=\begin{pmatrix} H_1 & V & & & \\ V^\dagger & H_2 & V & & \\ & V^\dagger & H_3 & V & \\ & & \ddots & \ddots & \ddots \end{pmatrix} \tag{8}$$

with the same matrices defined in Eq. (2). When $U_j=0$, the eigenenergies are given by

$$\varepsilon^{ABC}_{n,s}(p)=s\sqrt{(vp)^2+\gamma_1^2+2\gamma_1vp\cos\varphi_n}, \tag{9}$$

with $s=\pm$ and $\varphi_n(n=1,2,\ldots,N)$ being solutions of

$$vp\sin(N+1)\varphi+\gamma_1\sin N\varphi=0. \tag{10}$$

The corresponding wave function is $|\psi\rangle=\psi(A_1)|A_1\rangle+\psi(B_1)|B_1\rangle+\cdots$ with

$$\begin{pmatrix} \psi(A_j) \\ \psi(B_j) \end{pmatrix}=C\begin{pmatrix} e^{i\theta(j-1)}\sin(N+1-j)\varphi_n \\ se^{i\theta j}\sin j\varphi_n \end{pmatrix}, \tag{11}$$

where $\theta=\arctan p_y/p_x$ and C is a normalization factor. In the bulk limit, φ_n corresponds to the wave number along the layer stacking (z) direction. Actually, Eq. (10) is obtained by imposing a condition that a standing wave in z direction, composed by bulk wave functions, becomes zero at fictitious sites B_0 and A_{N+1} out of the system.

Equation (10) has N solutions of φ giving independent eigenstates. All of φ_n are real when $vp>\gamma_1N/(N+1)$, while only one becomes complex when $vp<\gamma_1N/(N+1)$, which corresponds to the evanescent mode in the bulk. In $vp\ll\gamma_1$, the complex branch approximates $e^{i\varphi}\approx -vp/\gamma_1$, giving the dispersion

$$\varepsilon \approx s\gamma_1(vp/\gamma_1)^N \tag{12}$$

with $s=\pm$. These are the only bands which appear at $\varepsilon=0$ and dominate the low-energy physics. The corresponding wave function is

$$\begin{pmatrix} \psi(A_j) \\ \psi(B_j) \end{pmatrix} \approx C \begin{pmatrix} e^{i\theta(j-1)}(-vp/\gamma_1)^{N+1-j} \\ se^{i\theta j}(-vp/\gamma_1)^j \end{pmatrix}. \tag{13}$$

The wave amplitude becomes largest on the top and bottom layers and decays exponentially inside, and thus is regarded as a surface state.[10] The wave function is exactly localized at the sites A_1 and B_N at $p=0$, and as p increases, the decay length increases as $-1/\log(vp/\gamma_1)$ in units of interlayer spacing d. In Fig. 4, we plot the band structures of *ABC* graphenes with $N=2$, 3, 5, 10, and 20, where the results of $U_j=0$ are indicated as black dotted curves. The surface states of Eq. (12) are shown as a pair of electron and hole bands touching at $\varepsilon=0$, which become flatter as N increases. The bilayer graphene (*AB*) can be regarded as $N=2$ of *ABA* family and also that of *ABC* family, and indeed, equally described either of Eq. (4) and (9).

When we consider the low-energy physics around zero energy, it is convenient to use the effective Hamiltonian reduced to the basis $|A_1\rangle, |B_N\rangle$.[7,15,47] In presence of U_j, it reads

$$\mathcal{H}_{ABC}^{(\mathrm{eff})} = \begin{pmatrix} U_1 & \gamma_1(vp_-/\gamma_1)^N \\ \gamma_1(vp_+/\gamma_1)^N & U_N \end{pmatrix}. \tag{14}$$

This approximation is valid when $vp/\gamma_1 \ll 1$, i.e., the actual wave function, Eq. (13), is well localized to A_1 or B_N. When we set the origin of potential as $U_1+U_N=0$, the eigenenergy is given by

$$\varepsilon_{s,p} = s\sqrt{\gamma_1^2(vp/\gamma_1)^{2N} + (\Delta U/2)^2}, \tag{15}$$

where $\Delta U = U_1 - U_N$ and $s=\pm$. The potential difference ΔU opens an energy gap between the valence and conduction bands.

III. SCREENING EFFECTS

A. Self-consistent treatment of screening effect

We compute the band structure of *ABA* or *ABC* multilayer graphenes in presence of gate electric field taking account of the screening effect. We consider undoped free-standing multilayer graphenes with an external electric field F_0 applied to the perpendicular direction. This situation can be realized in an experimental setup with an external top and bottom gates electrodes which are held at the opposite gate voltages with respect to the graphene.[18]

The potential at each layer, $U_j(j=1,2,\ldots,N)$ should be determined self-consistently. If a set of U_j is given, we can compute the band structure using Hamiltonian (1) for *ABA* or Eq. (8) for *ABC* multilayers. Then we determine the Fermi energy so that the total density is equal to n_{tot} (=0 in the present case), and calculate the electron density at each layer, $n_j(j=1,2,\ldots,N)$, from the occupied eigenstates. For screening effect, we consider the multilayer as parallel plates with zero thickness and respective electron densities n_j. The electric field between jth and $(j+1)$th layers is then given by

$$F_{(j,j+1)} = F_0 + \frac{e}{2\varepsilon}\left[\sum_{j'=1}^{j} n_{j'} - \sum_{j'=j+1}^{N} n_{j'}\right]. \tag{16}$$

Here ε is the permittivity of the interlayer spaces without the screening effect of π-band electrons, and we set $\varepsilon=2$ in the following calculations. Equation (16) immediately gives a new set of the electrostatic potential U_j, which should be identical to the initial U_j. To find the self-consistent solution, we employ an iterative numerical approach, where we start with $U_j=eF_0[j-(N+1)/2]$ as initial values and iterate the process until U_j's converge.

B. *ABA* multilayers

In Fig. 2(a), solid (red online) curves show the self-consistent band structures of *ABA* multilayers with several N's, in presence of the external field $eF_0d=0.2\gamma_1$. The original band structures at $F_0=0$ are also shown as dotted curves. In $N\geq 3$, we see that the lowest electron band is pulled down and the highest hole band is lifted up, making a band overlap around zero energy, as was previously recognized in the case of $N=3$ and 4.[18,26] The energy width of overlap becomes almost constant in $N\gtrsim 10$.

Figures 2(b) and 2(c) show the corresponding potential distribution U_j and electron density n_j, respectively, at the same external field $eF_0d=0.2\gamma_1$. In $N\geq 10$, we observe that the electric field (i.e., gradient in U_j) is screened within a few layers from the surface, leaving a triangular potential pocket at each end. The potential decay near the edge is almost identical between $N=10$ and 20. The overlapping bands observed in Fig. 2(a) are actually the bound states trapped at either of pockets; the states of the lowest electron and the highest hole bands are indeed localized at the potential minimum (left end) and maximum (right), respectively. Since E_F is zero, those bands are populated by electrons or holes, contributing to the most part of the screening field. A smooth decay observed in the electron density appears different from Ref. 50, which finds a charge oscillation with every second layer. We presume that this is due to the contribution from the intraband excitation, which was dropped in numerical calculations for neutral systems in Ref. 50.

The typical screening length λ_s (penetrating depth of electric field) can be roughly estimated by Thomas-Fermi approximation.[50] In this treatment, the potential decay on the surface is expressed as $U(z)\propto e^{-z/\lambda_s}$ with $\lambda_s=(e^2\rho_{3\mathrm{D}}/\varepsilon)^{-1/2}$, where $\rho_{3\mathrm{D}}$ is the three-dimensional density of states at the Fermi energy. For graphene, if we substitute $\rho_{3\mathrm{D}}=\bar{\rho}/d$ with $\bar{\rho}$ of Eq. (7), we obtain[50]

$$\lambda_s = \left(g_v g_s \frac{\gamma_1}{2\pi^2\hbar^2 v^2}\frac{e^2}{\varepsilon d}\right)^{-1/2}. \tag{17}$$

Using the parameters above, we get $\lambda_s \sim 1.3d \approx 0.43$ nm. In Fig. 2(b), we plot an exponential curve with decay length λ_s in Eq. (17) as a dotted curve to fit with the right half of the curve of $N=20$, which shows a fairly nice agreement. The depth of potential depth, or $|U(z=0)|$, is roughly estimated as $eF_0\lambda_s$, which determines the order of the energy width in band overlapping.

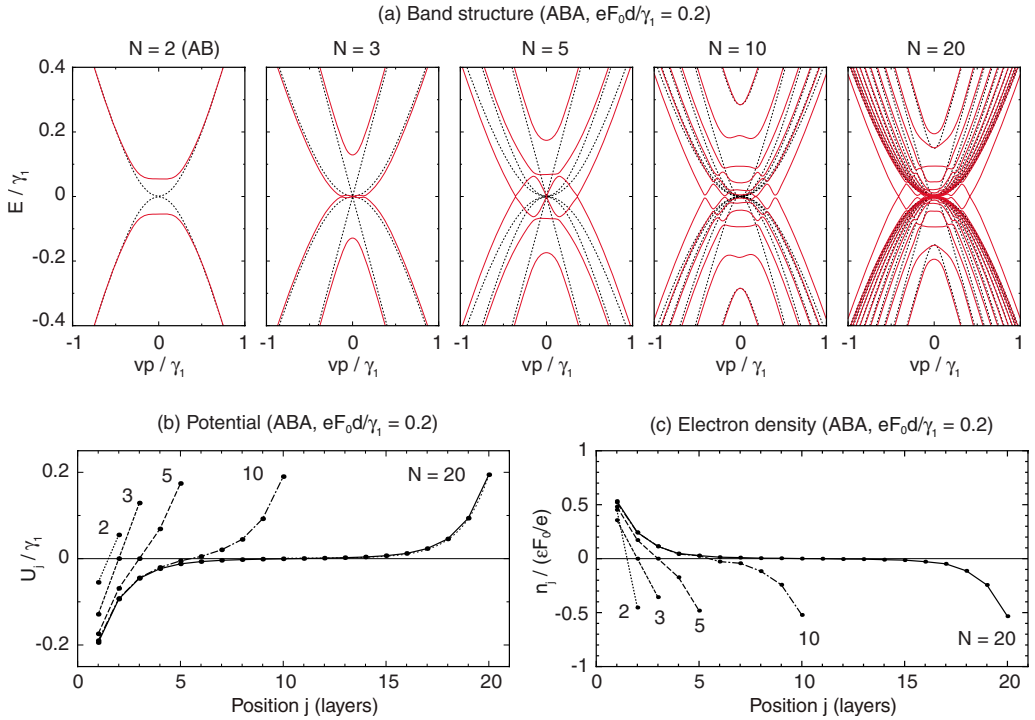

FIG. 2. (Color online) (a) Self-consistent band structures of *ABA* (Bernal) multilayer graphenes with several layer number N's at external field $eF_0d/\gamma_1=0.2$ (solid, red online) and 0 (dotted). (b) Potential distribution and (c) electron density of *ABA* multilayers with several N's at $eF_0d/\gamma_1=0.2$.

Figure 3 displays the potential difference $\Delta U=U_1-U_N$ as a function of the external field F_0. ΔU rises almost linearly in increasing F_0, except for a slight sublinear components in large F_0. This is consistent with Thomas-Fermi approximation since it gives linear screening in a weak external field.

C. *ABC* multilayers

The screening property of *ABC* multilayers is quite different from that of *ABA*, as the density of states diverges at $\varepsilon=0$ due to the flat band of the surface states. Before numerical calculations with full band model, we present an analytical approach using the effective 2×2 Hamiltonian of Eq. (14) valid in low energies. The potential difference ΔU between the top and bottom layers opens an energy gap between the valence and conduction bands, and thus only the lower band ($s=-$) is occupied when $n_{\rm tot}=0$. The density difference between the top and bottom layers, $\delta n=n(A_1)-n(B_N)$, is calculated as

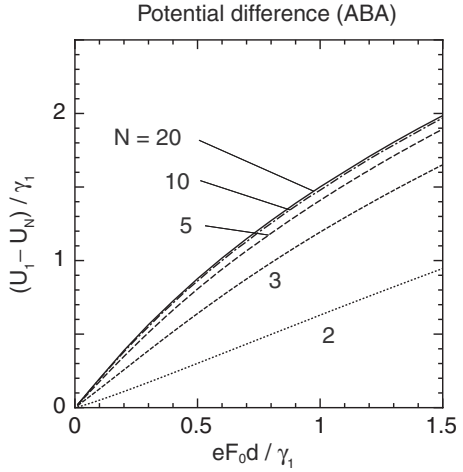

FIG. 3. Potential difference between outermost layers as a function of external field, in *ABA* multilayer graphenes with several N's.

$$\delta n=\frac{g_vg_s}{L^2}\sum_p|\psi_{-,p}(A_1)|^2-|\psi_{-,p}(B_N)|^2$$
$$=\frac{g_vg_s}{2\pi}\left(\frac{\gamma_1}{\hbar v}\right)^2\left(\frac{\Delta U}{2\gamma_1}\right)^{2/N}f_N, \tag{18}$$

where $[\psi_{-,p}(A_1),\psi_{-,p}(B_N)]$ is the eigenvector of Eq. (14) for $s=-$ band, and

$$f_N=\int_0^\infty\frac{tdt}{\sqrt{t^{2N}+1}}=\frac{\Gamma\left(\frac{1}{2}-\frac{1}{N}\right)\Gamma\left(1+\frac{1}{N}\right)}{2\sqrt{\pi}}, \tag{19}$$

with $\Gamma(x)$ the gamma function.

The density imbalance δn causes the screening field $F_{\rm ind}=-e\delta n/(2\varepsilon)$ opposed to the external field F_0, resulting in the total potential difference $\Delta U=e(F_0+F_{\rm ind})(N-1)d$. Together with Eq. (18), we obtain the self-consistent equation for ΔU,

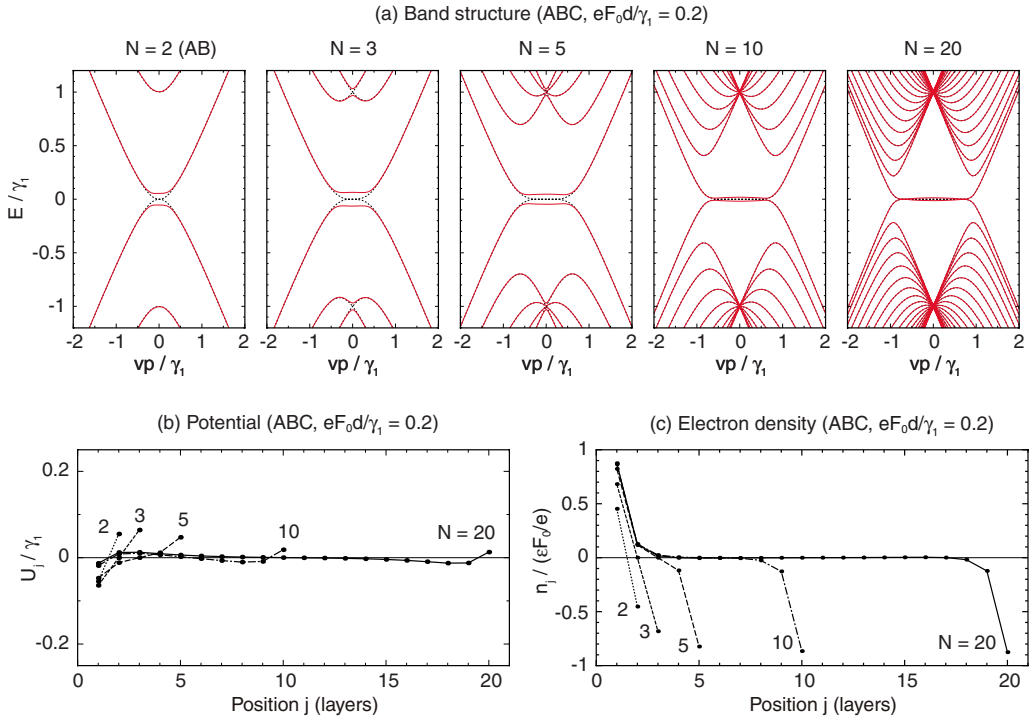

FIG. 4. (Color online) (a) Self-consistent band structures of *ABC* (rhombohedral) multilayer graphenes with several layer number N's at external field $eF_0d/\gamma_1=0.2$ (red, solid) and 0 (black, dotted). (b) Potential distribution and (c) electron density of *ABC* multilayers with several N's at $eF_0d/\gamma_1=0.2$.

$$\Delta U = e(N-1)d\left[F_0 - \frac{e}{2\varepsilon}\frac{g_v g_s}{2\pi}\left(\frac{\gamma_1}{\hbar v}\right)^2\left(\frac{\Delta U}{2\gamma_1}\right)^{2/N} f_N\right]. \tag{20}$$

In $N\geq 3$, ΔU is negligible compared to $\Delta U^{2/N}$ when ΔU is small enough. Then the equation is solved approximately as

$$\Delta U \approx 2\gamma_1 F_0^{N/2}\left[\frac{e}{2\varepsilon}\frac{g_v g_s}{2\pi}\left(\frac{\gamma_1}{\hbar v}\right)^2 f_N\right]^{-N/2}, \tag{21}$$

which is essentially nonlinear in F_0. In large-N limit, we have $f_N \approx 1/2$ and thus $\Delta U \approx 2\gamma_1(F_0/F_c)^{N/2}$, where $F_c = en_c/(2\varepsilon)$ is a characteristic field with an associated electron density

$$n_c = \frac{g_v g_s}{4\pi}\left(\frac{\gamma_1}{\hbar v}\right)^2 \approx 1.2\times 10^{13}\ \text{cm}^{-2}. \tag{22}$$

In increasing F_0, ΔU rapidly increases when the external field exceeds F_c.

n_c is the electron density accommodated in the flat-band region in large-N limit ($vp/\gamma_1<1$), i.e., the number of surface states. The field is completely screened in $F_0<F_c$ because the surface states are able to supply positive and negative charge to opposite surfaces to cancel the external field. The screening collapses at F_c when the density required for canceling exceeds the surface states population n_c.

$N=2$ (*AB*) is an exceptional in that the integration in Eq. (19) diverges logarithmically, giving infinite δn. Actually this is an artifact of the reduced 2×2 model due to the incorrect contributions from large p where the reduced Hamiltonian is not accurate. We can remove this by introducing a momentum cutoff $p_c \sim \gamma_1/v$, and get $f_{N=2}\sim(1/2)\log(\gamma_1/\Delta U)$. When we neglect the logarithmic dependence of f_N, ΔU becomes linear in F_0 in accordance with Eq. (20). The logarithmic factor gives a weak singularity at $\Delta U=0$.

Now we numerically calculate the self-consistent band structure of *ABC* multilayers using the full Hamiltonian (8). Figure 4(a) shows the results at $eF_0d=0.2\gamma_1$ (solid, red online) and 0 (dotted). In presence of the external field, an energy gap opens at low energy as expected. The gap width becomes smaller in $N>5$ in increasing N, suggesting a strong screening effect in large stacks. Figures 4(b) and 4(c) show the corresponding potential distribution U_j and the electron density n_j, respectively, at the same field $eF_0d=0.2\gamma_1$. At $N=20$, the potential is almost flat inside, as the external field is mostly screened by the electric charge on surface states localized at the outermost layers. This is in contrast with *ABA* multilayers, where an external field always penetrates inside with a few-layer thickness.

Figure 5 shows the plots of the potential difference $\Delta U=U_1-U_N$ as a function of the external field F_0. We actually observe nonlinear behavior expected in the analytical argument, where ΔU rapidly increases at $F_0\sim F_c$ (shown as a dashed vertical line). Lower panels in Fig. 5 compare the numerical results (solid) to the analytical expression (21) (dashed). We have nice agreements for $N\leq 5$ in small F_0 while the approximation becomes worse in large stack of $N\geq 10$. In large N's, the low-energy band almost reaches $vp/\gamma_1\sim 1$, where the wave function deeply penetrates into the bulk in accordance with Eq. (13). The finite penetration length makes the screening less effective, compared to the previous 2×2 model assuming the wave functions perfectly

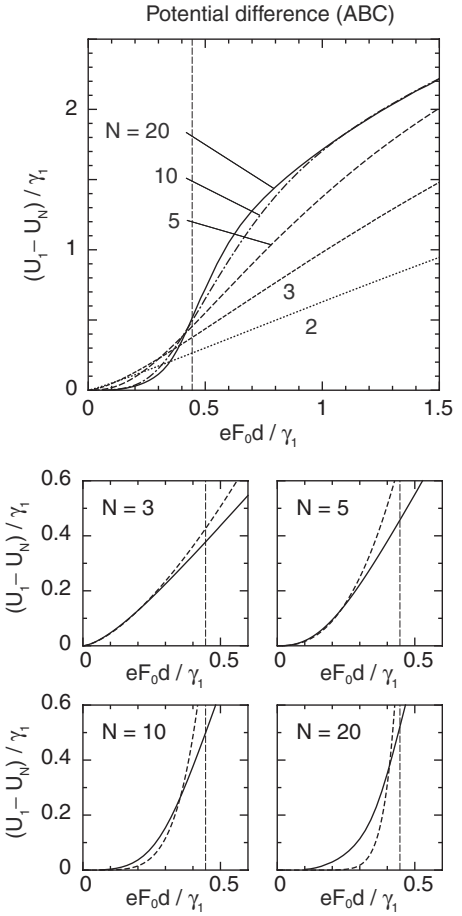

FIG. 5. Potential difference between outermost layers of *ABC* multilayers as a function of external field. Vertical broken line indicates the critical field F_c. Lower four panels compare the same results (solid curves) to the approximate expressions of Eq. (21) (dashed).

localized on the surface layers. As a result, numerical curves at large N's rise less sharply than the analytical ones as observed in Fig. 5. The wave penetration to the bulk is also responsible for Mexican hat structure[10] or narrowing of the gap around $vp/\gamma_1 \sim 1$ observed in Fig. 4(a). There the actual energy splitting becomes smaller than ΔU because the wave function is not perfectly localized at surface layers.

The width of the energy gap is an important quantity which can be detected experimentally. Figure 6 shows the gap width against the external field in the self-consistent band structures of *ABC* multilayers. In $N \leq 5$, the band bottom is approximately flat and the gap width therefore approximates ΔU (the splitting at $p=0$), and actually rises in proportional to $F_0^{N/2}$. In large stacks of $N \geq 10$, the energy gap becomes maximum around $F_0 \sim F_c$, and is suppressed in greater F_0's, due to the gap narrowing at $vp/\gamma_1 \sim 1$.

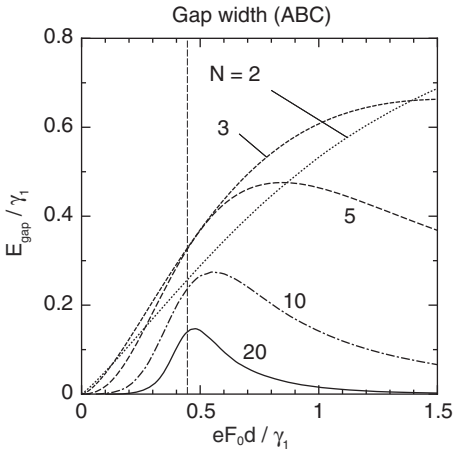

FIG. 6. Energy gap width in the self-consistent band structures as function of external field for *ABC* multilayers with several N's. Vertical broken line indicates the critical field F_c.

IV. CONCLUSION

We studied electronic band structures of *ABA* and *ABC* graphene multilayers in the presence of an perpendicular electric field including the screening effect. In *ABA* multilayers, the electric field produces band overlapping accompanying a linear screening well described by the Thomas-Fermi approximation. In *ABC* multilayers, in contrast, the surface-state bands dominating low energies cause a strong nonlinear screening effect through opening an energy gap.

While in the present model we only include the primary parameters γ_0 and γ_1 in our model, the extra band parameters corresponding to the further hopping generally affect the band structure of multilayer graphenes.[36,38–42] In *ABC* graphenes, it was shown that the extra parameters gives a fine structure to the surface band, of which energy scale is expected to be on the order of 10 meV.[49] We expect that the screening property would be influenced by those effects when the external potential is as small as those energy scales. As another remark, the electron-electron interaction other than the screening effect may create nontrivial ground states in a flat band such as in *ABC* multilayers, while we leave those problems for future works.

ACKNOWLEDGMENTS

The author thanks E. McCann and T. Ando for helpful discussions. This work was supported in part by Grant-in-Aid for Scientific Research on Priority Area "Carbon Nanotube Nanoelectronics" and by Grant-in-Aid for Scientific Research from Ministry of Education, Culture, Sports, Science and Technology Japan.

[1] K. S. Novoselov, A. K. Geim, S. V. Morozov, D. Jiang, Y. Zhang, S. V. Dubonos, I. V. Grigorieva, and A. A. Firsov, Science **306**, 666 (2004).
[2] K. S. Novoselov, A. K. Geim, S. V. Morozov, D. Jiang, M. I. Katsnelson, I. V. Grigorieva, S. V. Dubonos, and A. A. Firsov, Nature (London) **438**, 197 (2005).
[3] Y. Zhang, Y.-W. Tan, H. L. Stormer, and P. Kim, Nature (London) **438**, 201 (2005).
[4] K. S. Novoselov, E. McCann, S. V. Morozov, V. I. Fal'ko, M. I. Katsnelson, U. Zeitler, D. Jiang, F. Schedin, and A. K. Geim, Nat. Phys. **2**, 177 (2006).
[5] T. Ohta, A. Bostwick, T. Seyller, K. Horn, and E. Rotenberg, Science **313**, 951 (2006).
[6] T. Ohta, A. Bostwick, J. L. McChesney, T. Seyller, K. Horn, and E. Rotenberg, Phys. Rev. Lett. **98**, 206802 (2007).
[7] E. McCann and V. I. Fal'ko, Phys. Rev. Lett. **96**, 086805 (2006).
[8] M. Koshino and T. Ando, Phys. Rev. B **73**, 245403 (2006).
[9] J. Nilsson, A. H. Castro Neto, F. Guinea, and N. M. R. Peres, Phys. Rev. Lett. **97**, 266801 (2006).
[10] F. Guinea, A. H. Castro Neto, and N. M. R. Peres, Phys. Rev. B **73**, 245426 (2006).
[11] S. Latil and L. Henrard, Phys. Rev. Lett. **97**, 036803 (2006).
[12] C. L. Lu, C. P. Chang, Y. C. Huang, J. M. Lu, C. C. Hwang, and M. F. Lin, J. Phys.: Condens. Matter **18**, 5849 (2006); C. L. Lu, C. P. Chang, Y. C. Huang, R. B. Chen, and M. L. Lin, Phys. Rev. B **73**, 144427 (2006).
[13] B. Partoens and F. M. Peeters, Phys. Rev. B **74**, 075404 (2006); **75**, 193402 (2007).
[14] M. Koshino and T. Ando, Phys. Rev. B **76**, 085425 (2007).
[15] J. L. Mañes, F. Guinea, and M. A. H. Vozmediano, Phys. Rev. B **75**, 155424 (2007).
[16] M. Koshino and T. Ando, Phys. Rev. B **77**, 115313 (2008).
[17] M. Koshino and T. Ando, Solid State Commun. **149**, 1123 (2009).
[18] M. Koshino and E. McCann, Phys. Rev. B **79**, 125443 (2009).
[19] A. A. Avetisyan, B. Partoens, and F. M. Peeters, Phys. Rev. B **79**, 035421 (2009).
[20] A. A. Avetisyan, B. Partoens, and F. M. Peeters, Phys. Rev. B **80**, 195401 (2009).
[21] J. Güttinger, C. Stampfer, F. Molitor, D. Graf, T. Ihn, and K. Ensslin, New J. Phys. **10**, 125029 (2008).
[22] M. F. Craciun, S. Russo, M. Yamamoto, J. B. Oostinga, A. F. Morpurgo, and S. Tarucha, Nat. Nanotechnol. **4**, 383 (2009).
[23] E. McCann, Phys. Rev. B **74**, 161403(R) (2006).
[24] E. McCann, D. S. L. Abergel, and V. I. Fal'ko, Solid State Commun. **143**, 110 (2007).
[25] H. Min, B. R. Sahu, S. K. Banerjee, and A. H. MacDonald, Phys. Rev. B **75**, 155115 (2007).
[26] M. Aoki and H. Amawashi, Solid State Commun. **142**, 123 (2007).
[27] P. Gava, M. Lazzeri, A. M. Saitta, and F. Mauri, Phys. Rev. B **79**, 165431 (2009).
[28] E. V. Castro, K. S. Novoselov, S. V. Morozov, N. M. R. Peres, J. M. B. Lopes dos Santos, J. Nilsson, F. Guinea, A. K. Geim, and A. H. Castro Neto, Phys. Rev. Lett. **99**, 216802 (2007).
[29] J. B. Oostinga, H. B. Heersche, X. Liu, A. F. Morpurgo, and L. M. K. Vandersypen, Nature Mater. **7**, 151 (2008).
[30] Z. Q. Li, E. A. Henriksen, Z. Jiang, Z. Hao, M. C. Martin, P. Kim, H. L. Stormer, and D. N. Basov, Phys. Rev. Lett. **102**, 037403 (2009).
[31] L. M. Zhang, Z. Q. Li, D. N. Basov, M. M. Fogler, Z. Hao, and M. C. Martin, Phys. Rev. B **78**, 235408 (2008).
[32] A. B. Kuzmenko, E. van Heumen, D. van der Marel, P. Lerch, P. Blake, K. S. Novoselov, and A. K. Geim, Phys. Rev. B **79**, 115441 (2009).
[33] Y. Zhang, T.-T. Tang, C. Girit, Z. Hao, M. C. Martin, A. Zettl, M. F. Crommie, Y. R. Shen, and F. Wang, Nature (London) **459**, 820 (2009).
[34] K. F. Mak, C. H. Lui, J. Shan, and T. F. Heinz, Phys. Rev. Lett. **102**, 256405 (2009).
[35] H. Lipson and A. R. Stokes, Proc. R. Soc. London **A181**, 101 (1942).
[36] P. R. Wallace, Phys. Rev. **71**, 622 (1947).
[37] J. W. McClure, Phys. Rev. **104**, 666 (1956).
[38] J. W. McClure, Phys. Rev. **108**, 612 (1957).
[39] J. C. Slonczewski and P. R. Weiss, Phys. Rev. **109**, 272 (1958).
[40] J. W. McClure, Phys. Rev. **119**, 606 (1960).
[41] G. Dresselhaus and M. S. Dresselhaus, Phys. Rev. **140**, A401 (1965).
[42] M. S. Dresselhaus and G. Dresselhaus, Adv. Phys. **51**, 1 (2002).
[43] R. R. Haering, Can. J. Phys. **36**, 352 (1958).
[44] J. W. McClure, Carbon **7**, 425 (1969).
[45] C. L. Lu, H. C. Lin, C. C. Hwang, J. Wang, M. F. Lin, and C. P. Chang, Appl. Phys. Lett. **89**, 221910 (2006).
[46] C. L. Lu, C. P. Chang, Y. C. Huang, J. H. Ho, C. C. Hwang, and M. F. Lin, J. Phys. Soc. Jpn. **76**, 024701 (2007).
[47] H. Min and A. H. MacDonald, Phys. Rev. B **77**, 155416 (2008).
[48] D. P. Arovas and F. Guinea, Phys. Rev. B **78**, 245416 (2008).
[49] M. Koshino and E. McCann, Phys. Rev. B **80**, 165409 (2009).
[50] F. Guinea, Phys. Rev. B **75**, 235433 (2007).
[51] H. Miyazaki, S. Odaka, T. Sato, S. Tanaka, H. Goto, A. Kanda, K. Tsukagoshi, Y. Ootuka, and Y. Aoyagi, Appl. Phys. Express **1**, 034007 (2008).
[52] N. J. Lee, J. W. Yoo, Y. J. Choi, C. J. Kang, D. Y. Jeon, D. C. Kim, S. Seo, and H. J. Chung, Appl. Phys. Lett. **95**, 222107 (2009).
[53] Y. Sui and J. Appenzeller, Nano Lett. **9**, 2973 (2009).